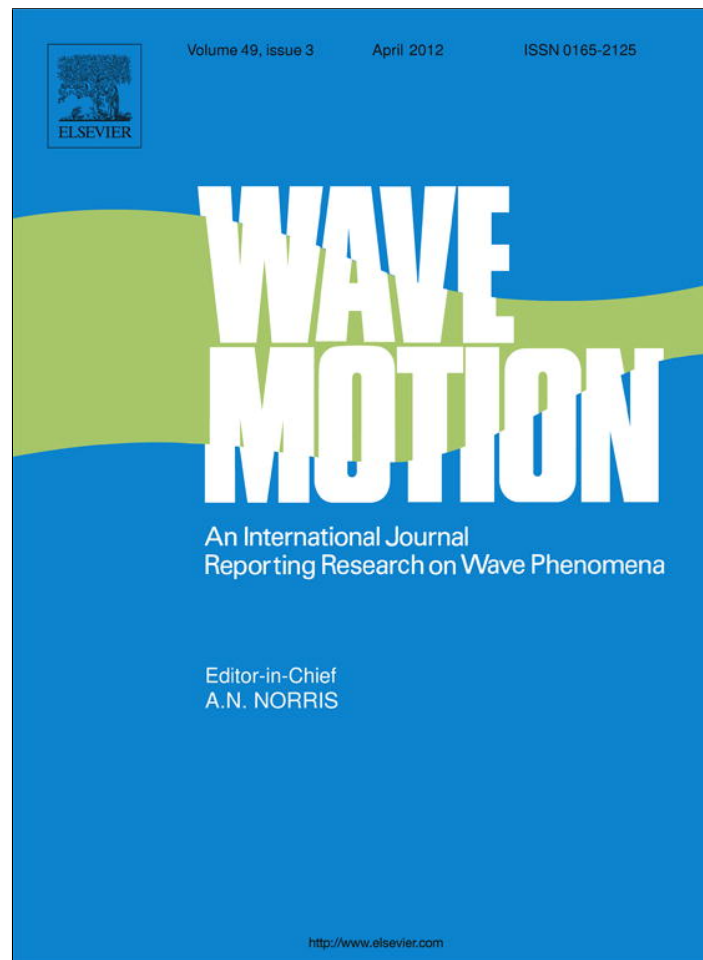


Provided for non-commercial research and education use.
Not for reproduction, distribution or commercial use.



This article appeared in a journal published by Elsevier. The attached copy is furnished to the author for internal non-commercial research and education use, including for instruction at the authors institution and sharing with colleagues.

Other uses, including reproduction and distribution, or selling or licensing copies, or posting to personal, institutional or third party websites are prohibited.

In most cases authors are permitted to post their version of the article (e.g. in Word or Tex form) to their personal website or institutional repository. Authors requiring further information regarding Elsevier's archiving and manuscript policies are encouraged to visit:

<http://www.elsevier.com/copyright>



Contents lists available at SciVerse ScienceDirect

Wave Motion

journal homepage: www.elsevier.com/locate/wavemoti

Multi-displacement microstructure continuum modeling of anisotropic elastic metamaterials

A.P. Liu^{a,b}, R. Zhu^b, X.N. Liu^{a,b}, G.K. Hu^{a,*}, G.L. Huang^{b,*}

^a School of Aerospace Engineering, Beijing Institute of Technology, Beijing, 100081, China

^b Department of Systems Engineering, University of Arkansas at Little Rock, AR, 72204, USA

ARTICLE INFO

Article history:

Received 6 July 2011

Received in revised form 30 October 2011

Accepted 26 December 2011

Available online 8 January 2012

Keywords:

Metamaterial

Multi-displacement

Continuum

Anisotropic mass density

Wave propagation

ABSTRACT

An elastic metamaterial made of lead cylinders coated with elliptical rubbers in an epoxy matrix is considered, and its anisotropic effective dynamic mass density tensor is numerically determined and demonstrated. To capture both dipolar resonant motion and microstructure deformation in the composite, a new multi-displacement microstructure continuum model is proposed. In the formulation, additional displacement and kinematic variables are introduced to describe global and local deformations, respectively. The macroscopic governing equations of the two-dimensional anisotropic elastic metamaterial are explicitly derived through a simplified procedure. To verify the current model, wave dispersion curves from the current model are compared with those from the finite element simulation for both longitudinal and transverse waves. Very good agreement is observed in both the acoustic and optic wave modes. This work could provide a benchmark of continuum modeling of elastic metamaterials with nonelementary microstructures.

© 2011 Elsevier B.V. All rights reserved.

1. Introduction

Metamaterials are a new class of ordered composites that exhibit exceptional electromagnetic, optic and mechanical properties not readily observed in nature [1,2]. Although electromagnetic (EM) and acoustic metamaterials have been studied intensively, elastic metamaterials have received much less attention, despite the fact that elastic metamaterials offer richer behaviors as they enable both longitudinal and transverse waves to propagate. Various novel concepts and engineering applications of elastic metamaterials have been successfully demonstrated such as mechanical filters, sound and vibration isolators, elastic waveguides and energy harvesting [3–8].

To understand global wave mechanism in elastic metamaterials, the most important and efficient approach is homogenization. For isotropic elastic metamaterials, conventional homogenization will result in three independent effective parameters: effective mass density, effective bulk modulus and effective shear modulus. Until now, several homogenization methods have been developed to model this kind of materials as effective homogeneous elastic media. Those methods include the plane wave expansion (PWE) technique, the coherent potential approximation (CPA), the micromechanics analytical model or multiple scattering theory (MST) based on the long-wavelength limit [9–16]. By requiring only the wavelength in the matrix to be much larger than the size of the microstructures, the extension of the CPA or effective medium theory (EMT) was further developed to predict the effective properties of the elastic metamaterials [17]. However, these analytical methods are mainly based on the analytical scattering solution of microstructures with simple geometries (sphere or cylinder). To achieve the desirable effective properties, elastic metamaterials with complex microstructures or

* Corresponding authors.

E-mail addresses: hugeng@bit.edu.cn (G.K. Hu), glhuang@ualr.edu (G.L. Huang).

microstructure arrangements must be designed. For nonelementary microstructure geometries, an exact analytical model is not practicable and computational techniques should be suggested such as the multiple multipole (MMP) method [18], lumped mass method [19], and finite difference method [20]. For the acoustic metamaterial, the anisotropic effective mass density can be achieved by changing position or distribution array of the microstructure in the unit cell [21,22]. However, for the elastic metamaterial, the microstructure geometry should be properly designed to obtain the anisotropic effective mass density [23–26]. A 2D elastic resonator of arbitrary geometry was systematically studied through a finite element modal analysis [27]. Gu et al. [28] investigated local resonance modes of elliptic cylinders coated with silicon rubber in a rigid matrix to obtain the anisotropic effective mass density. However, most of these methods mainly focus on an understanding of the local resonant mechanism. Practically, one may want to predict dynamic behavior of the elastic metamaterial by using an effective continuum model, wherein effects of the microstructure are included in effective properties and/or in macro-dynamics equations. The obtained macro-dynamics equations can be applied to problems of time-dependent vibration and transit wave propagation in the finite and infinite structures, which is important for potential engineering applications of metamaterial devices. However, continuum homogenization of elastic metamaterials with complex microstructures is a challenging task.

Until now, few efforts have been made to study the effective properties beyond the quasi-static limit or in higher frequency regions, although some interesting wave phenomena occur only when the wavelength is comparable to the lattice scale. To describe wave propagation problems with wavelengths in an order of dimensions of microstructures, Wozniak [29] proposed a non-asymptotic approach of the macro-dynamics modeling of composite. Milton and Willis [30] and Milton [31] presented a rigorous theoretical foundation for the dynamic effective parameters of the elastic metamaterial beyond the quasi-static limit. The microscale effects due to non-local behavior were explained by the modification of linear continuum elastodynamic equations. Similar efforts have been made through work on metamaterials with a macroscopic higher order gradient or non-local elastic response [32]. An alternative approach is to employ additional kinematic variables to describe the nonhomogeneous local deformation in the microstructure of the solid. This approach leads to Cosserat continuum models [33,34] or micropolar models [35,36] or strain gradient theory [37] or the microstructure continuum theory [38,39]. Microstructure continuum theory has recently been adopted to describe global dynamic behavior of isotropic elastic metamaterials with discrete microstructures (a mass-spring system) [40]. Accuracy of the model was verified by comparison with the results obtained from the finite element method. However, the microstructure continuum model or high-order continuum model has difficulty in capturing the dipolar motion, in which the inner inclusion moves out of phase with respect to motion of the matrix in elastic metamaterials. Additional displacement variables are needed to capture the dipolar motion.

In this paper, the anisotropic dynamic mass density tensor of an elastic metamaterial made of lead cylinders coated with elliptical rubbers in an epoxy matrix is first numerically determined. To analytically obtain global governing equations of motion in the elastic metamaterial, the complex continuous microstructure is simplified to a discrete mass-spring system based on strain energy equivalence. Based on the simplified system, a new multi-displacement microstructure continuum theory is developed to capture both dipolar local resonant motion and microstructure deformation by introducing both multi-displacement variables and micro-deformation variables, which are not considered in the conventional continuum model. The developed model is verified and applied to investigate global wave propagation in 2D anisotropic elastic metamaterials under the plane stress assumption.

2. Anisotropic elastic metamaterials

In this study, an anisotropic elastic metamaterial made of heavy cylinder cores coated with elliptical soft layer and embedded in a matrix is considered, as shown in Fig. 1(a), and its representative volume element (RVE) is identified in Fig. 1(b). The microstructure is distributed in a rectangular lattice array. In the figure, the hard inclusion core is labeled as medium 1, the soft coating medium is labeled as medium 2, and the matrix is labeled as medium 3. The isotropic material constants of the inclusion core, the coating layer and the matrix are ρ_1, E_1, ν_1 ; ρ_2, E_2, ν_2 and ρ_3, E_3, ν_3 , respectively. The radius of the core is a . The lattice constants along the X_2 and X_3 directions are denoted as d_2 and d_3 . The semimajor and semiminor axes of the ellipse are denoted as b_1 and b_2 , respectively. In the unit cell (k, l) , the position of the center point is given in the global coordinate $X_2 = X_2^l$ and $X_3 = X_3^k$. For convenience, we define a local polar coordinate system (r, θ) as well as a local Cartesian coordinates (x_2, x_3) in the unit cell with $x_2 = r \cos \theta$ and $x_3 = r \sin \theta$, as shown in Fig. 1(b). Strong anisotropic properties of the metamaterial along the X_2 and X_3 directions can be achieved by adjusting dimensions of the major and minor axes of the coating ellipse.

Due to geometric complexity of the microstructure, analytical-based methods cannot be applied directly for the determination of the effective dynamic mass density [28]. In this study, a numerical-based method will be adopted [8]. Consider the unit cell in Fig. 1(b), time-harmonic displacements $u_\alpha = \hat{u}_\alpha e^{i\omega t}$ with $\alpha = 2, 3$ are prescribed on the exterior boundary, and a harmonic analysis of the unit cell is performed by using the finite element method (FEM), from which resultant forces $F_\alpha = \hat{F}_\alpha e^{i\omega t}$ on the exterior boundary can be obtained. The effective mass density tensor can then be numerically defined and determined by

$$\begin{Bmatrix} \hat{F}_2 \\ \hat{F}_3 \end{Bmatrix} = -\omega^2 A_c \begin{bmatrix} \rho_{22}^{eff} & \rho_{23}^{eff} \\ \rho_{32}^{eff} & \rho_{33}^{eff} \end{bmatrix} \begin{Bmatrix} \hat{u}_2 \\ \hat{u}_3 \end{Bmatrix} \quad (1)$$

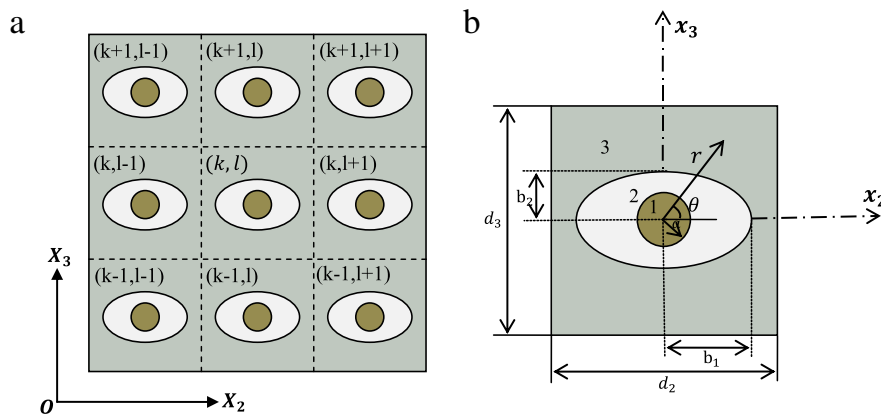


Fig. 1. (a) An anisotropic elastic metamaterial made of cylinders coated with elliptical soft layer in a matrix; (b) The (k, l) element (RVE).

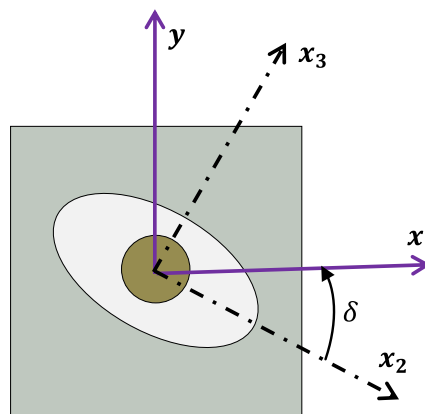


Fig. 2. Coordinate systems of the unit cell with an arbitrary direction.

Table 1

The microstructure geometry parameters.

Lattice parameters	Elliptical coat (mm)	Circle coat (mm)
$d_2 = d_3$	20	20
a	3	5.155
b_1	7	7.14
b_2	5	7.14

where $A_c = d_2 d_3$ is the area of the unit cell. To demonstrate that the mass density follows the coordinate transformation law, an effective mass density tensor in an arbitrary coordinate system (x, y) , as shown in Fig. 2, is similarly determined. In the figure, (x_2, x_3) is a rectangular Cartesian coordinate system in principal directions and (x, y) is an arbitrary Cartesian coordinate system. It should be mentioned that the unit cell in Fig. 2 is specifically suggested for simplification of numerical calculation, in which the outer matrix seems to follow the unit cell transformation. This is because the outer host matrix is mainly functioned as an effective mass in the calculation of the effective mass density of the unit cell. Therefore, determination of the effective mass density is independent on the outer matrix geometry. Based on the numerical results of the unit cell, it can be proved that the effective mass density follows the coordinate transformation law as

$$\begin{bmatrix} \rho_{xx}^{eff} & \rho_{xy}^{eff} \\ \rho_{yx}^{eff} & \rho_{yy}^{eff} \end{bmatrix} = \begin{bmatrix} C^2 \rho_{22}^{eff} + S^2 \rho_{33}^{eff} & CS(\rho_{33}^{eff} - \rho_{22}^{eff}) \\ CS(\rho_{33}^{eff} - \rho_{22}^{eff}) & C^2 \rho_{33}^{eff} + S^2 \rho_{22}^{eff} \end{bmatrix} \quad (2)$$

where $C = \cos \delta$, $S = \sin \delta$, and δ is the angle of the transformation. Therefore, the effective mass density admits the second-order tensorial property.

Fig. 3 shows the effective mass density of the elastic metamaterial along a direction $\delta = 30^\circ$ by using the FEM model, where $\rho_{ave} = (\rho_1 A_1 + \rho_2 A_2 + \rho_3 A_3) / A_c$ is the average static mass density for the composite. The microstructure geometry parameters and the constituent material parameters are given in Tables 1 and 2, respectively. From the figure, we can clearly see that the effective mass density is frequency-dependent, anisotropic ($\rho_{xx}^{eff} \neq \rho_{yy}^{eff}$, $\rho_{xy}^{eff} \neq 0$) and becomes negative around the resonant frequency. For the metamaterial with the current microstructure, two different resonant frequencies along x_2 and x_3 directions can be found as $f^{*1} = 862$ Hz and $f^{*2} = 950$ Hz, respectively, which indicate anisotropy of the

Table 2
The constituent material parameters.

The parameters	Core: lead	Coating: rubber	Matrix: epoxy
Mass density	$\rho_1 : 11.31 \times 10^3 \text{ kg/m}^3$	$\rho_2 : 0.92 \times 10^3 \text{ kg/m}^3$	$\rho_3 : 1.11 \times 10^3 \text{ kg/m}^3$
Young's modulus	$E_1 : 1.3 \times 10^{10} \text{ N/m}^2$	$E_2 : 1.5 \times 10^6 \text{ N/m}^2$	$E_3 : 2.35 \times 10^9 \text{ N/m}^2$
Poisson's ratio	$\nu_1 : 0.435$	$\nu_2 : 0.499$	$\nu_3 : 0.38$
Area	$A_1 : \pi a^2$	$A_2 : \pi (b_1 b_2 - a^2)$	$A_3 : d_2 d_3 - \pi b_1 b_2$

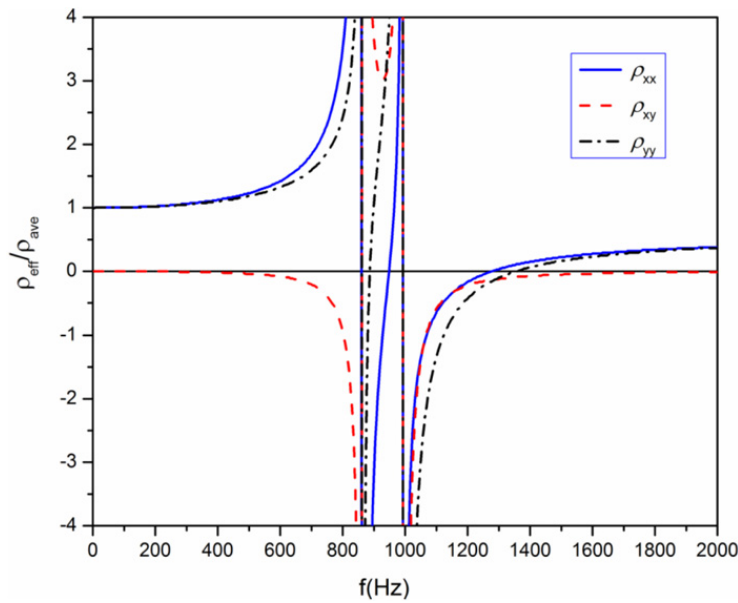


Fig. 3. The anisotropic effective mass density of the elastic metamaterial predicted by the FEM model along a direction $\delta = 30^\circ$.

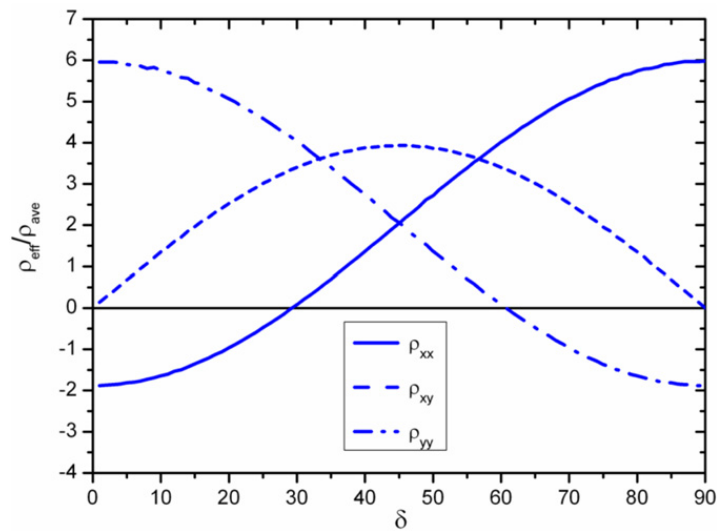


Fig. 4. The effective mass density with respect to the angle δ .

metamaterial. The significant difference between ρ_{xx}^{eff} and ρ_{yy}^{eff} can be observed when the frequency is close to the resonant frequency. It is also interesting to note that the mass density become isotropic ($\rho_{xx}^{eff} = \rho_{yy}^{eff}, \rho_{xy}^{eff} = 0$) when the frequency is much less or much larger than the resonant frequency. Effective mass density for a 2D ternary phononic crystal with two resonators was also discussed by Gu et al. [28].

Fig. 4 shows the effective mass densities in functions of the angle δ at frequency $f = 950 \text{ Hz}$. The strong anisotropy of the effective mass density can be clearly found ($\rho_{xx}^{eff} \neq \rho_{yy}^{eff}, \rho_{xy}^{eff} \neq 0$) with the angle change of the incident wave. It should be emphasized that the anisotropy of the effective mass density can be tuned by adjusting the geometry of the microstructure.

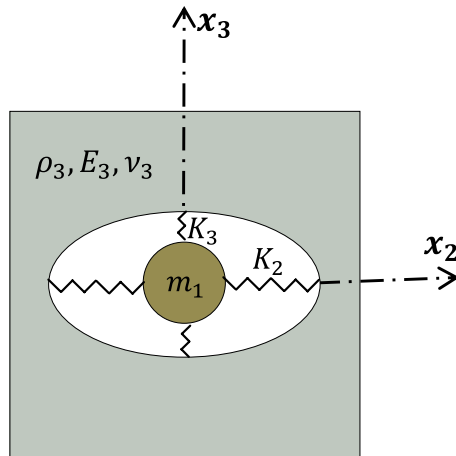


Fig. 5. The equivalent RVE for the (k, l) element of the elastic metamaterial.

3. Multi-displacement microstructure continuum modeling of the elastic metamaterial

In the previous section, the anisotropic effective mass density tensor of the elastic metamaterial and its mechanism are calculated and determined through the numerical analysis, from which the anisotropic negative mass density is illustrated. However, in order to understand global dynamic behavior of the elastic metamaterial, an analytical-based continuum model is needed to properly describe the dispersive behavior as well as band-gap behavior. The obtained macro-dynamics equations can be applied directly to dynamic problems of the elastic metamaterial with the finite and infinite structures, which is important for its potential engineering applications. In this section, a multi-displacement microstructure continuum model will be developed analytically for the first time. First, the analytical effective mass density tensor of the elastic metamaterial will be determined through a simplified model. Then additional displacement and kinematic variables will be introduced to capture the local dipolar motion and microstructure deformation.

3.1. A simplified model of the elastic metamaterial

For the elastic metamaterial with the complicated microstructure geometry, analytical-based homogenization approaches have difficulties in finding the exact local scattering wave field. In this study, the RVE with the continuous microstructure is first simplified to the RVE with a discrete mass-spring microstructure with spring constants K_2 and K_3 , as shown in Fig. 5 [30], based on the strain energy equivalence between the two systems. The inclusion core is reduced as a rigid mass $m_1 = \rho_1 \pi a^2$ and the coating material is replaced by the springs with the spring constants K_2 and K_3 because of the large stiffness mismatch between the core and the coating material. The spring constants K_2 and K_3 can be numerically determined as $K_\alpha = F_\alpha / \gamma_\alpha$ with $\alpha = 2, 3$, where F_α is the restoring force on the outer fixed boundary of the coating layer and $u_\alpha = \gamma_\alpha$ is the applied displacement along x_2 and x_3 directions of the coating layer. For the general geometry of the coating layer, the problem can be numerically solved by using the finite element method (FEM).

Based on the analytical Lorentz model [30], four components of the effective density tensor of the composite system in Fig. 5 along principal direction can be obtained analytically as

$$\begin{bmatrix} \rho_{22}^{eff} & \rho_{23}^{eff} \\ \rho_{32}^{eff} & \rho_{33}^{eff} \end{bmatrix} = \frac{1}{A_c} \begin{bmatrix} m_3 + \frac{2m_1 K_2}{2K_2 - m_1 \omega^2} & 0 \\ 0 & m_3 + \frac{2m_1 K_3}{2K_3 - m_1 \omega^2} \end{bmatrix} \quad (3)$$

where $A_c = d_2 d_3$ is the area of the RVE, and $m_3 = \rho_3 A_3$ is the mass of the matrix in a RVE. The density tensor in an arbitrary coordinate system (x, y) can be easily determined according to the second-order tensorial property. Fig. 6 shows a comparison of the effective mass density of the anisotropic elastic metamaterial with the microstructure along the direction $\delta = 30^\circ$ from the numerical model and the current analytical Lorentz model. For the elliptical coat geometric parameters in Table 1, the spring constants can be obtained as $K_2 = 4.93 \times 10^6$ kg/m and $K_3 = 6.45 \times 10^6$ kg/m. Very good agreement between these two models can be clearly observed, which substantiates the fact that the simplified discrete mass-spring model can be used as the dynamic equivalent system of the anisotropic elastic metamaterial in Fig. 1. A small difference around the resonant frequencies between the two models is because the discrete Lorentz model ignores the mass of the coating layer and assumes the matrix to be rigid.

3.2. A multi-displacement microstructure continuum model

In this subsection, a new homogeneous high-order continuum theory will be proposed to homogenize the simplified elastic anisotropic metamaterial, as shown in Fig. 7. For the elastic metamaterial, the inner mass will move out-of-phase

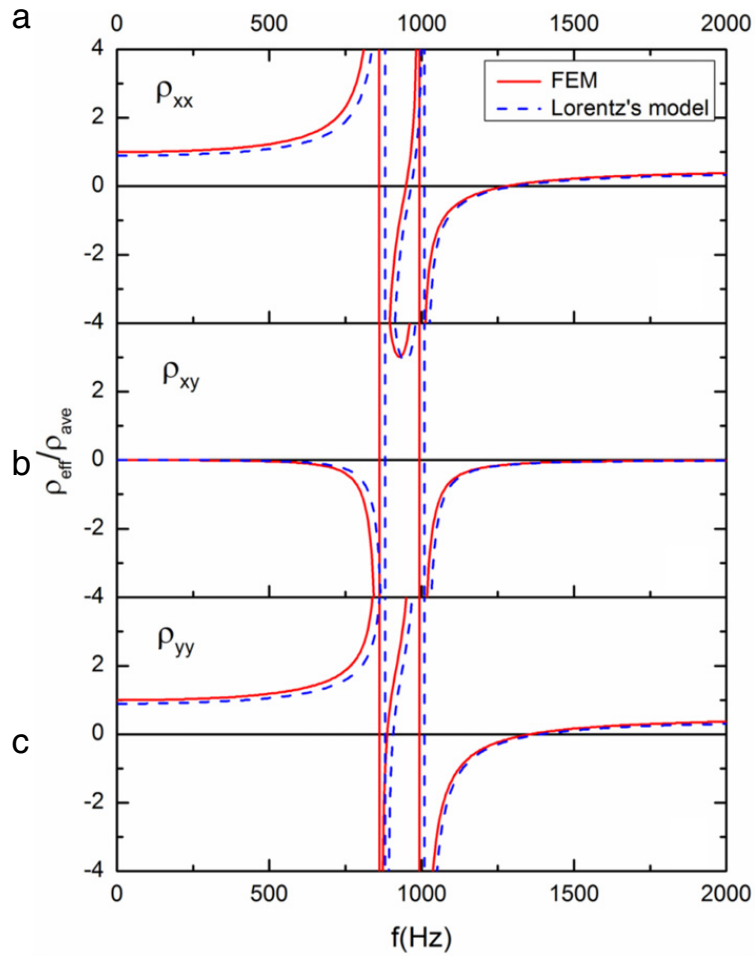


Fig. 6. Comparison of the effective mass density predicted by the FEM model and the analytical Lorentz model.

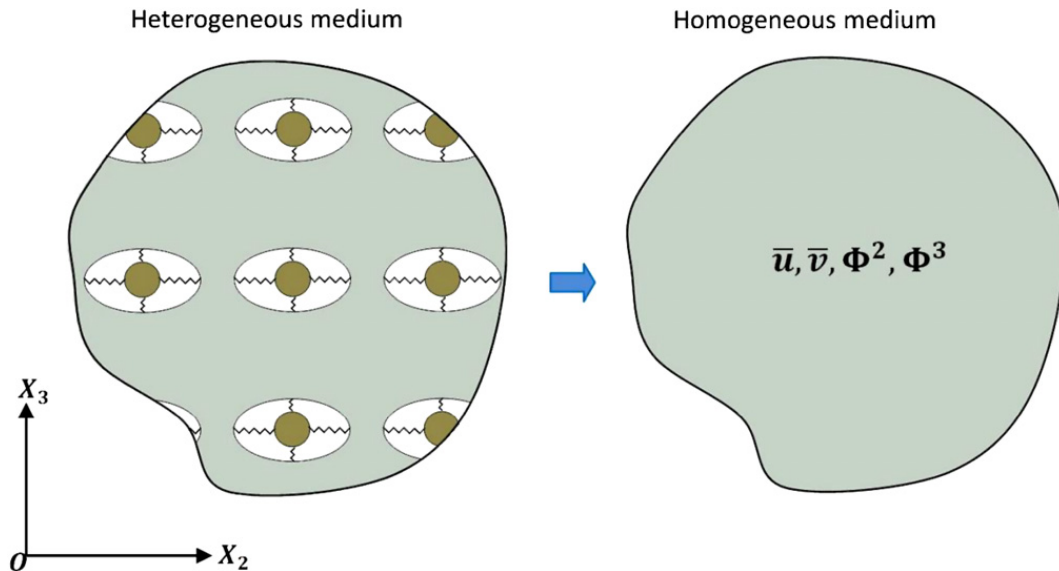


Fig. 7. Heterogeneous medium replaced by a homogeneous medium.

with respect to the motion of the composite when the frequency is close to the resonant frequency of the inner mass, which is called the dipolar motion. The schematic illustration of the dipolar motion in the elastic metamaterial near the resonant frequency is shown in Fig. 8.

The conventional continuum model cannot capture the dipolar motion, therefore, a continuum model with additional multi-displacement variables should be introduced. Specifically, attention is also paid to the problem with wavelengths

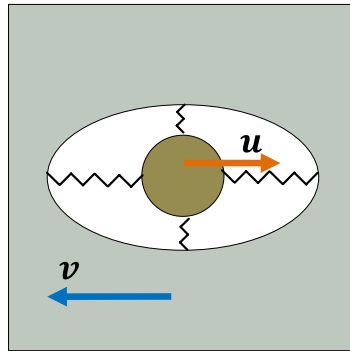


Fig. 8. A schematic illustration of dipolar motion in the metamaterial near the resonant frequency.

in an order of the dimension of the unit-cell. To describe the relative high-frequency dynamic behaviors, microstructure kinetic variables are also needed. In the formulation, we assume the lead core is rigid because of its high modulus and the local displacements in the matrix can be approximated by linear series expansions in terms of quantities which are defined at the center of the element. The micro-deformations are assumed as follows:

- (1) In the inclusion of the cell (k, l) , $(r < a)$

$$\mathbf{u}^1 = \bar{\mathbf{u}} \tag{4a}$$

- (2) In the matrix of the cell (k, l) , $(r \geq \bar{b})$

$$\mathbf{u}^3 = \bar{\mathbf{v}} + \bar{b}\boldsymbol{\Phi}^2\boldsymbol{\Theta} + (r - \bar{b})\boldsymbol{\Phi}^3\boldsymbol{\Theta} \tag{4b}$$

where

$$\begin{aligned} \mathbf{u}^1 &= \begin{bmatrix} u_2^{1(k,l)} & u_3^{1(k,l)} \end{bmatrix}^T, & \bar{\mathbf{u}} &= \begin{bmatrix} \bar{u}_2^{(k,l)} & \bar{u}_3^{(k,l)} \end{bmatrix}^T, \\ \mathbf{u}^3 &= \begin{bmatrix} u_2^{3(k,l)} & u_3^{3(k,l)} \end{bmatrix}^T, & \bar{\mathbf{v}} &= \begin{bmatrix} \bar{v}_2^{(k,l)} & \bar{v}_3^{(k,l)} \end{bmatrix}^T, & \boldsymbol{\Theta} &= \begin{bmatrix} \cos \theta & \sin \theta \end{bmatrix}^T, \\ \boldsymbol{\Phi}^2 &= \begin{bmatrix} \phi_{22}^{2(k,l)} & \phi_{32}^{2(k,l)} \\ \phi_{23}^{2(k,l)} & \phi_{33}^{2(k,l)} \end{bmatrix}, & \boldsymbol{\Phi}^3 &= \begin{bmatrix} \phi_{22}^{3(k,l)} & \phi_{32}^{3(k,l)} \\ \phi_{23}^{3(k,l)} & \phi_{33}^{3(k,l)} \end{bmatrix}, & \bar{b} &= \frac{b_1 b_2}{\sqrt{b_1^2 \sin^2 \theta + b_2^2 \cos^2 \theta}}. \end{aligned}$$

where $\bar{\mathbf{u}}, \bar{\mathbf{v}}, \boldsymbol{\Phi}^2$ and $\boldsymbol{\Phi}^3$ are global variables in functions of (X_2, X_3, t) , the local displacements \mathbf{u}^1 and \mathbf{u}^3 are functions of (X_2, X_3, x_2, x_3, t) , or in other words, functions of (X_2, X_3, r, θ, t) . Physical interpretation of the terms in Eq. (4) is that global displacements $\bar{\mathbf{u}}$ and $\bar{\mathbf{v}}$ are the displacements of the center of the inclusion and the center of the matrix, respectively; while $\boldsymbol{\Phi}^2$ represents micro-deformation in the area within the inner boundary of the matrix, and $\boldsymbol{\Phi}^3$ represents micro-deformation in the matrix. It should be mentioned that the additional displacement components are necessary to capture the dipolar motion in the metamaterial, which is different from the microstructure continuum theory [39]. In the microstructure continuum theory, additional microstructure variables were only introduced to capture the micro-deformation in the microstructure.

In principle, the boundary condition between the unit-cell and the neighboring cells should be satisfied on every point of the boundaries. However, the approximated local field, assumed in Eq. (4b), cannot exactly satisfy the point-to-point continuity at the boundaries. In this study, relaxation boundary continuity conditions, which are defined as averaged displacement continuity conditions at the interfaces of the cells, are suggested as:

$$\int_{-d_2/2}^{d_2/2} \left[u_\alpha^{3(k+1,l)} \Big|_{x_3=-\frac{d_3}{2}} - u_\alpha^{3(k,l)} \Big|_{x_3=\frac{d_3}{2}} \right] dx_2 = 0 \tag{5a}$$

$$\int_{-d_3/2}^{d_3/2} \left[u_\alpha^{3(k,l+1)} \Big|_{x_2=-\frac{d_2}{2}} - u_\alpha^{3(k,l)} \Big|_{x_2=\frac{d_2}{2}} \right] dx_3 = 0 \tag{5b}$$

where $u_\alpha^{3(k+1,l)}$ and $u_\alpha^{3(k,l+1)}$ represent displacement components of the matrix in the cells $(k + 1, l)$ and $(k, l + 1)$. Eq. (5a) represents the averaged displacement continuity on the boundary between the cell (k, l) and the cell $(k + 1, l)$; and Eq. (5b) represents the averaged displacement continuity on the boundary between the cell (k, l) and the cell $(k, l + 1)$. This approximate is much more reasonable for relatively low frequency cases. Substituting the local displacement in the matrix Eq. (4b) into Eq. (5a) results in

$$\begin{aligned} \bar{v}_\alpha^{(k+1,l)} - \bar{v}_\alpha^{(k,l)} - \frac{b_1 d_3}{d_2} \ln \left(\frac{1 + \sqrt{1 + \xi^2}}{\xi} \right) & \left(\phi_{3\alpha}^{2(k+1,l)} - \phi_{3\alpha}^{3(k+1,l)} + \phi_{3\alpha}^{2(k,l)} - \phi_{3\alpha}^{3(k,l)} \right) \\ & - \frac{d_3}{2} \left(\phi_{3\alpha}^{3(k+1,l)} + \phi_{3\alpha}^{3(k,l)} \right) = 0 \end{aligned} \quad (6a)$$

where $\xi = \frac{b_1 d_3}{b_2 d_2}$.

Similarly, another continuous condition can be obtained from Eq. (5b) as

$$\begin{aligned} \bar{v}_\alpha^{(k,l+1)} - \bar{v}_\alpha^{(k,l)} - \frac{b_2 d_2}{d_3} \ln \left(\xi + \sqrt{1 + \xi^2} \right) & \left(\phi_{2\alpha}^{2(k,l+1)} - \phi_{2\alpha}^{3(k,l+1)} + \phi_{2\alpha}^{2(k,l)} - \phi_{2\alpha}^{3(k,l)} \right) \\ & - \frac{d_2}{2} \left(\phi_{2\alpha}^{3(k,l+1)} + \phi_{2\alpha}^{3(k,l)} \right) = 0. \end{aligned} \quad (6b)$$

The corresponding local strain in the matrix can be obtained as

$$\mathbf{e}^3 = \nabla \otimes \mathbf{u}^3 \quad (7)$$

where ∇ is the differentiation operator in the local coordinate system (x_2, x_3) , $\mathbf{e}^3 = \begin{bmatrix} \varepsilon_{22}^{3(k,l)} & \varepsilon_{23}^{3(k,l)} \\ \varepsilon_{32}^{3(k,l)} & \varepsilon_{33}^{3(k,l)} \end{bmatrix}$ is the strain tensor of the matrix and its components are given in Appendix A.

Based on the displacement expressions in Eq. (4), the total kinetic energy density in the cell (k, l) can be calculated as

$$T_{ave}^{(k,l)} = \frac{1}{A_c} (T^{1(k,l)} + T^{3(k,l)}) \quad (8)$$

where $T^{1(k,l)}$ and $T^{3(k,l)}$ are the kinetic energies in the inclusion and matrix, respectively.

On the other hand, the strain deformation energy in the spring within the cell (k, l) can be obtained as

$$\begin{aligned} W^{s(k,l)} = K_2 & \left[\left(\bar{v}_2^{(k,l)} - \bar{u}_2^{(k,l)} \right)^2 + \left(b_1 \phi_{22}^{2(k,l)} \right)^2 + \left(b_1 \phi_{32}^{2(k,l)} \right)^2 \right] \\ & + K_3 \left[\left(\bar{v}_3^{(k,l)} - \bar{u}_3^{(k,l)} \right)^2 + \left(b_2 \phi_{33}^{2(k,l)} \right)^2 + \left(b_2 \phi_{23}^{2(k,l)} \right)^2 \right] \end{aligned} \quad (9)$$

and the strain deformation energy in the matrix for the plane stress problem is

$$W^{m(k,l)} = \frac{E_3}{2(1 - \nu_3^2)} \iint_{A_3} \left[\left(\varepsilon_{22}^{3(k,l)} \right)^2 + \left(\varepsilon_{33}^{3(k,l)} \right)^2 + 2\nu_3 \left(\varepsilon_{22}^{3(k,l)} \right) \left(\varepsilon_{33}^{3(k,l)} \right) + 2(1 - \nu_3) \left(\varepsilon_{23}^{3(k,l)} \right)^2 \right] dA_3. \quad (10)$$

The total strain deformation energy averaged over the volume of cell (k, l) yields

$$W_{ave}^{(k,l)} = \frac{1}{A_c} (W^{s(k,l)} + W^{m(k,l)}). \quad (11)$$

To obtain a continuum model, we now introduce fields that are continuous in the global coordinate system X_2 and X_3 , and the values at $X_2 = X_2^l$ and $X_3 = X_3^k$ coincide with those in the actual micro (local) field variables at the center of the cell. Therefore, we can consider the strain energy density $W(X_2, X_3, t)$ and the kinetic energy density $T(X_2, X_3, t)$ as continuous functions. Based on Eq. (8), the kinetic energy density $T(X_2, X_3, t)$ in the continuum field is

$$T(X_2, X_3, t) = T_{ave}^{(k,l)} = \frac{1}{A_c} (T^{1(k,l)} + T^{3(k,l)}) \quad (12)$$

and the strain energy density $W(X_2, X_3, t)$ is

$$W(X_2, X_3, t) = W_{ave}^{(k,l)} = \frac{1}{A_c} (W^{s(k,l)} + W^{m(k,l)}) \quad (13)$$

where energy densities $T(X_2, X_3, t)$ and $W(X_2, X_3, t)$ are given in Appendix B.

At the same time, the continuity conditions in Eq. (6) can be written in the terms of continuous variables by considering the field variables as continuous functions of X_2 and X_3 , as

$$\begin{aligned} S_{3\alpha}(X_2, X_3, t) = \frac{\partial \bar{v}_\alpha}{\partial X_3} - \frac{2b_1}{d_2} \ln \left(\frac{1 + \sqrt{1 + \xi^2}}{\xi} \right) & \left(\phi_{3\alpha}^2 - \phi_{3\alpha}^3 + \frac{d_3}{2} \frac{\partial \phi_{3\alpha}^2}{\partial X_3} - \frac{d_3}{2} \frac{\partial \phi_{3\alpha}^3}{\partial X_3} \right) \\ & - \phi_{3\alpha}^3 - \frac{d_3}{2} \frac{\partial \phi_{3\alpha}^3}{\partial X_3} = 0 \end{aligned} \quad (14a)$$

and

$$S_{2\alpha}(X_2, X_3, t) = \frac{\partial \bar{v}_\alpha}{\partial X_2} - \frac{2b_2}{d_3} \ln(\xi + \sqrt{1 + \xi^2}) \left(\phi_{2\alpha}^2 - \phi_{2\alpha}^3 + \frac{d_2}{2} \frac{\partial \phi_{2\alpha}^2}{\partial X_2} - \frac{d_2}{2} \frac{\partial \phi_{2\alpha}^3}{\partial X_2} \right) - \phi_{2\alpha}^3 - \frac{d_2}{2} \frac{\partial \phi_{2\alpha}^3}{\partial X_2} = 0 \quad (14b)$$

where $\alpha = 2, 3$.

Considering a fixed regular region V of the medium, the displacement equations of motion can be obtained by employing Hamilton's principle for independent variables in V and a specified time interval $t_0 \leq t \leq t_1$ as

$$\delta \int_{t_0}^{t_1} \int_V F dt dV + \int_{t_0}^{t_1} \delta W_1 dt = 0 \quad (15)$$

where $F = T - W$, δW_1 is the variation of the work done by external forces, and dV is the scalar volume element. For the current model, there are no existing external forces and the continuity conditions can be considered as subsidiary conditions through the use of Lagrangian multipliers, so the problem can be redefined as

$$\delta \int_{t_0}^{t_1} \int_V F dt dV = 0 \quad (16)$$

with

$$F = T - W - \sum_{\alpha=2}^3 (\Gamma_{2\alpha} S_{2\alpha} + \Gamma_{3\alpha} S_{3\alpha}) \quad (17)$$

where the Lagrangian multipliers $\Gamma_{2\alpha}$ and $\Gamma_{3\alpha}$ are functions of X_2, X_3 and t . Since the function F as given in Eq. (17) depends only on the global field variables (X_2, X_3, t) and their first order derivatives, the system of the Euler equations can be written as

$$\sum_{r=1}^3 \frac{\partial}{\partial p_r} \left[\frac{\partial F}{\partial \left(\frac{\partial f_s}{\partial p_r} \right)} \right] - \frac{\partial F}{\partial f_s} = 0 \quad (18)$$

where f_s ($s = 1, 2, \dots, 16$) represent the sixteen dependent variables $\bar{u}_\alpha, \bar{v}_\alpha, \phi_{2\alpha}^2, \phi_{3\alpha}^2, \phi_{2\alpha}^3, \phi_{3\alpha}^3, \Gamma_{2\alpha}$ and $\Gamma_{3\alpha}$ ($\alpha = 2, 3$); and p_r ($r = 1, 2, 3$) are the spatial variables X_2, X_3 and time variable t . A system of sixteen governing equations of motion can be obtained from the Eq. (18), which is given in Appendix C.

4. Numerical simulation and discussions

4.1. Model verification

To verify the proposed continuum model, let us first consider a two-dimensional elastic metamaterial with a cylinder heavy core coated with a circular soft layer and embedded in matrix in a square lattice array. The microstructure geometry parameters are listed in Table 1 and the material parameters are provided in Table 2. Based on the simplified model for the continuous systems, spring constants for the 2D plane stress problem with the circle coated metamaterial can be numerically determined as $K_2 = K_3 = 1.184 \times 10^7$ N/m. It should be mentioned that for the current microstructure geometry, when the coating material is incompressible (the Poisson's ratio of the coat material ν_2 is about 0.5), the analytical solution for the spring constants [41] is also available as $K_2 = K_3 \cong \frac{40\pi\mu_2(a^2+b^2)}{25(a^2+b^2)\ln(b/a) - 9(b^2-a^2)}$, where μ_2 is the shear modulus of the coating material $\mu_2 = \frac{E_2}{2(1+\nu_2)}$. The good agreement about the spring constant's prediction between the two methods shows the accuracy of the current numerical method.

For a longitudinal wave propagation along X_2 direction in the metamaterial with infinite dimension in X_3 direction, the available kinematic variables include multi-displacement variables \bar{u}_2, \bar{v}_2 , the microstructure field variables ϕ_{22}^2, ϕ_{22}^3 and the Lagrangian multiplier Γ_{22} . Therefore, five governing equations can be obtained as

$$\rho_1 A_1 \ddot{\bar{u}}_2 + 2K_2 (\bar{u}_2 - \bar{v}_2) = 0 \quad (19)$$

$$\rho_3 A_3 \ddot{\bar{v}}_2 + 2K_2 (\bar{v}_2 - \bar{u}_2) - A_c \frac{\partial \Gamma_{22}}{\partial X_2} = 0 \quad (20)$$

$$\begin{aligned} & \rho_3 J_1 \ddot{\phi}_{22}^2 + \rho_3 (J_{60} - J_1) \ddot{\phi}_{22}^3 + 2b^2 K_2 \phi_{22}^2 + \frac{E_3}{1 - \nu_3^2} [J_4 (\phi_{22}^2 - \phi_{22}^3) + J_7 \phi_{22}^3] \\ & + \frac{E_3}{2(1 + \nu_3)} [J_6 (\phi_{22}^2 - \phi_{22}^3)] - A_c \frac{2b}{d_3} \ln(\xi + \sqrt{1 + \xi^2}) \Gamma_{22} + A_c \frac{bd_2}{d_3} \ln(\xi + \sqrt{1 + \xi^2}) \frac{\partial \Gamma_{22}}{\partial X_2} = 0 \end{aligned} \quad (21)$$

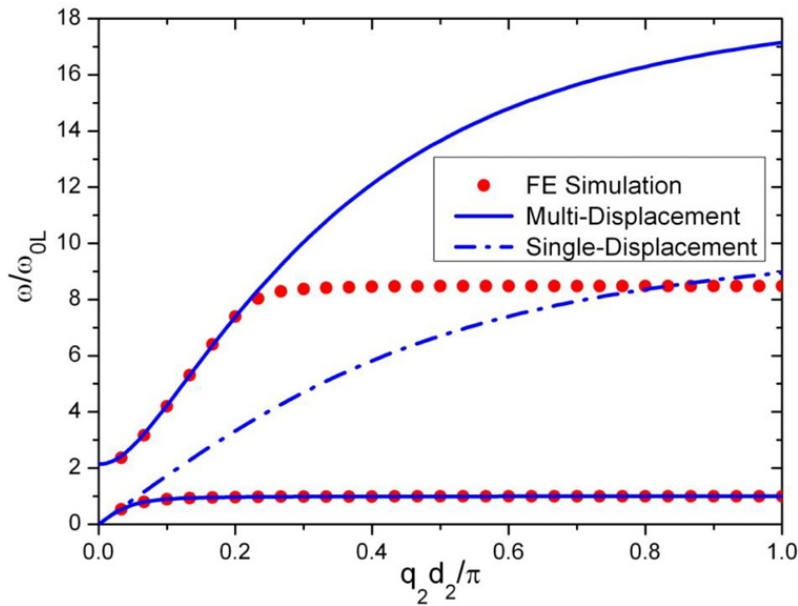


Fig. 9. Comparison of the normalized dispersion curves by the current model, the reduced single-displacement model and the FE simulation for longitudinal wave propagation.

$$\begin{aligned} & \rho_3 (J_1 + I_3^m - 2J_{60}) \ddot{\phi}_{22}^3 + \rho_3 (J_{60} - J_1) \ddot{\phi}_{22}^2 + \frac{E_3}{1 - \nu_3^2} [A_3 \phi_{22}^3 + J_4 (\phi_{22}^3 - \phi_{22}^2)] \\ & + J_7 \phi_{22}^2 - 2J_7 \phi_{22}^3 + \frac{E_3}{2(1 + \nu_3)} [J_6 (\phi_{22}^3 - \phi_{22}^2)] + A_c \left[\frac{2b}{d_3} \ln(\xi + \sqrt{1 + \xi^2}) - 1 \right] \Gamma_{22} \\ & - A_c \left[\frac{bd_2}{d_3} \ln(\xi + \sqrt{1 + \xi^2}) - \frac{d_2}{2} \right] \frac{\partial \Gamma_{22}}{\partial X_2} = 0 \end{aligned} \quad (22)$$

$$\frac{\partial \bar{v}_2}{\partial X_2} - \frac{2b}{d_3} \ln(\xi + \sqrt{1 + \xi^2}) \left(\phi_{22}^2 - \phi_{22}^3 + \frac{d_2}{2} \frac{\partial \phi_{22}^2}{\partial X_2} - \frac{d_2}{2} \frac{\partial \phi_{22}^3}{\partial X_2} \right) - \phi_{22}^3 - \frac{d_2}{2} \frac{\partial \phi_{22}^3}{\partial X_2} = 0 \quad (23)$$

where $\xi = \frac{d_3}{d_2}$ for the circle-coated elastic metamaterial. For the longitudinal wave propagating in the X_2 direction, the continuum wave fields can be defined as

$$\{\bar{u}_2, \bar{v}_2, \phi_{22}^2, \phi_{22}^3, \Gamma_{22}\} = \{B_1, B_2, B_3, B_4, B_5\} \exp[i(q_2 X_2 - \omega t)] \quad (24)$$

where $i = \sqrt{-1}$, B_1, B_2, B_3, B_4 and B_5 are constant amplitudes, q_2 is the wave-number in the X_2 direction, and ω is the angular frequency. Substitution of (24) into the Eqs. (19)–(23) yields five homogeneous equations for B_1, B_2, B_3, B_4 and B_5 . For a nontrivial set of solutions the determinant of the coefficients must vanish to yield the dispersion relation. The exact wave dispersion curves can also be calculated by using commercial finite element (FE) software, ANSYS 11.0. In the FE model, Plane-82 element is used to model the elastic medium, and Mass-21 and Combine-14 elements are used to model the spring-mass system. After properly applying boundary conditions for the model, modal analysis is conducted to obtain the natural frequencies, from which the dispersion curve can be obtained. Fig. 9 shows comparison of the normalized dispersion curves of the longitudinal wave predicted by the current multi-displacement microstructure continuum model, the reduced single-displacement continuum model, and the FE simulation, where $\omega_{0L} = \sqrt{2K_2/m_1} = 5007.37$ rad/s and the resonant frequency is $f_{0L} = \omega_{0L}/(2\pi) = 797$ Hz. The single-displacement model is reduced from the current model by removing the additional global displacement variable. It is found that the multi-displacement microstructure continuum model can give an excellent prediction for the acoustic wave mode and is also reasonably good for the optic wave mode for $q_2 d_2 < 0.9$. The band gap behavior of the elastic metamaterial can be accurately predicted by using the current model, which is very useful for the design of the desirable elastic metamaterial. It is also very interesting to note that the band gap behavior cannot be captured when only a single-displacement (conventional) continuum model is adopted. This is understandable because no additional degrees of freedom are used to capture the local dipolar resonance phenomenon. In addition, it is noticed that the current model has difficulty to capture the optic wave mode when the frequency is around $\omega/\omega_{0L} = 8.48$ ($f = 6757$ Hz). Based on the eigenmode analysis at this frequency, it can be found that the resonance deformation is focus on the coating layer and no motions occur in the core and host matrix, which is similar to the quadrupolar resonance. To capture the quadrupolar resonance in the metamaterial, additional microstructure kinematic variables in the coating layer may be needed.

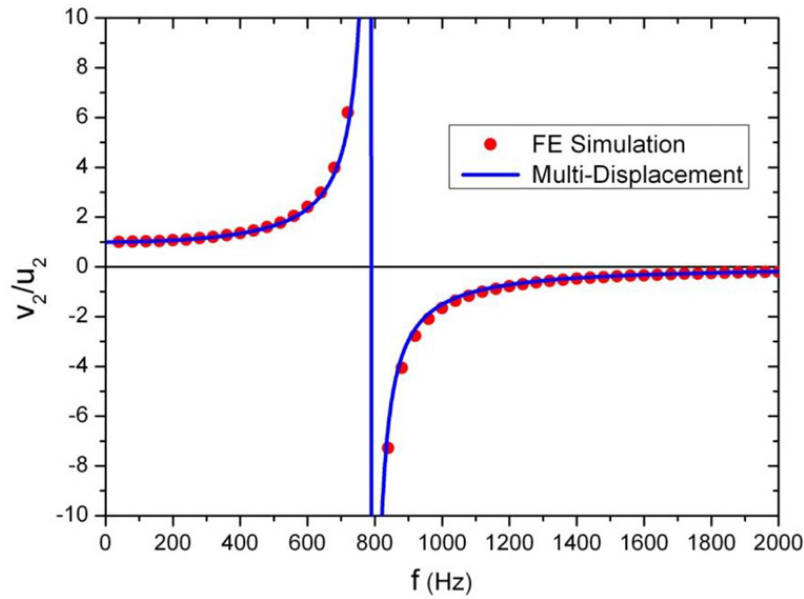


Fig. 10. The displacement amplitude ratio of the matrix to the core in function of the frequency.

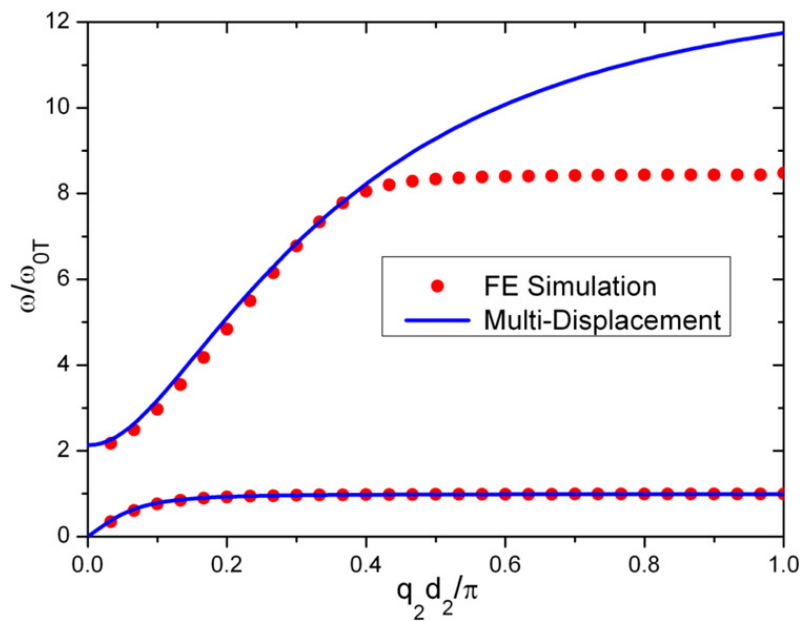


Fig. 11. Comparison of the normalized dispersion curves obtained by the current model and the FE simulation for transverse wave propagation.

Fig. 10 shows the wave amplitude ratio of the matrix to the core in a function of the frequency predicted by the current model and the finite element method (FEM). The very good agreement between the current model and FEM is observed for the local displacement prediction in the elastic metamaterial, which is impossible for the conventional continuum models. Around $f = 797$ Hz, there exists a resonance in the metamaterial in which the displacement of the core is very large and experience a very sharp change from the in-phase state to the out-of-phase state. A large displacement ratio enhancement can be observed in the in-phase resonance region. From eigenmode analysis, we can find that the core inclusion moves opposite to the motion in the matrix in the band gap frequency range, which cannot be captured through the conventional continuum model.

Fig. 11 shows a comparison of the normalized dispersion curves predicted by the current model and the FE simulation for transverse shear wave propagation. The material constants are the same as those used in Fig. 9, where $\omega_{0T} = \sqrt{2K_3/m_1} = 5007.37$ rad/s = ω_{0L} for the isotropic elastic metamaterial. The very reasonable agreement between the current model and the FE simulation is also observed for both the acoustic wave mode and the optic wave mode. Also, it is noticed that the current model is invalid to capture the quadrupolar resonant mechanism when the frequency is around $\omega/\omega_{0L} = 8.48$ ($f = 6757$ Hz).

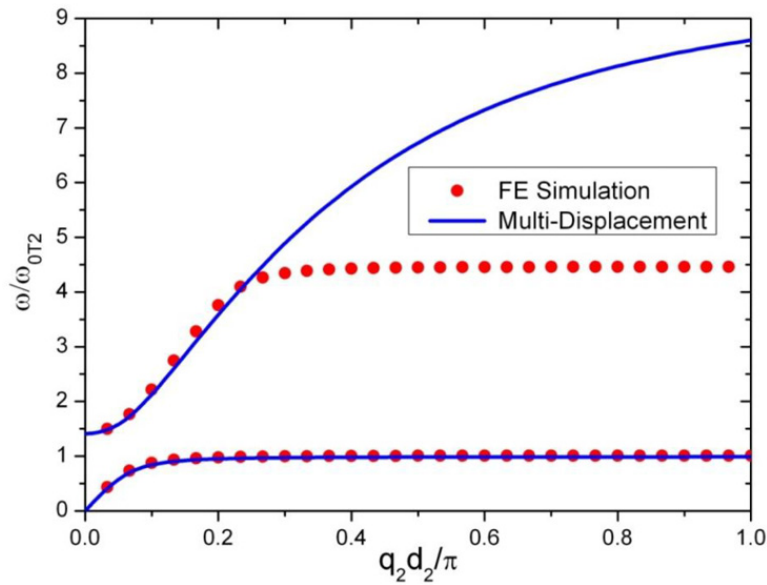


Fig. 12. Comparison of the normalized dispersion curves for the anisotropic metamaterial for transverse wave propagation along X_2 direction.

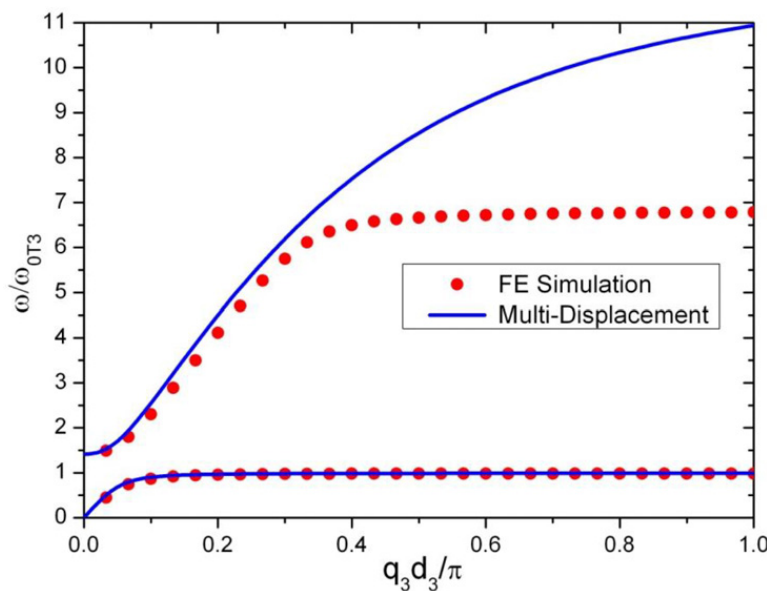


Fig. 13. Comparison of the normalized dispersion curves for the anisotropic metamaterial for transverse wave propagation along X_3 direction.

4.2. Wave propagation in anisotropic elastic metamaterials

It is well known that for isotropic metamaterials, wave propagation behavior is identical for any wave propagation direction. For anisotropic elastic metamaterials, wave propagation behavior is different along different directions and is direction-dependent. Figs. 12 and 13 show the comparison of the normalized dispersion curves for the transverse shear wave propagation along X_2 and X_3 directions for the anisotropic elastic metamaterial, respectively. In the figures, the material properties are the same as in Table 2. The microstructure geometry parameters are shown in Table 1 with an elliptical coating medium, from which the spring constants are numerically obtained as $K_2 = 4.93 \times 10^6$ kg/m, $K_3 = 6.45 \times 10^6$ kg/m. The resonant angular frequencies are $\omega_{0T2} = \sqrt{2K_3/m_1}$ and $\omega_{0T3} = \sqrt{2K_2/m_1}$, respectively. It is found that the current model can provide good prediction of dispersion curves for both the acoustic wave mode and the optic wave mode along different wave propagation directions. The anisotropic wave propagation behavior can be observed from the different wave dispersion curves along different directions. From the numerical simulation, it is also concluded that the band gap frequency regime is within the same frequency when the effective mass density becomes negative, which confirms wave mechanism in the current anisotropic metamaterial is caused by the dipolar wave motion.

5. Conclusions

In this paper, an anisotropic elastic metamaterial made of lead cylinders coated with elliptical rubbers in an epoxy matrix is considered. An anisotropic effective mass density tensor is first numerically determined. To describe global dynamic behavior in the elastic metamaterial, a new multi-displacement microstructure continuum model is developed to obtain the macroscopic governing equations of the anisotropic elastic metamaterial. The current model is verified through comparison of wave dispersion curves predicted by the current model and the finite element simulation for both longitudinal and transverse shear waves. Very good agreement is observed in both the acoustic and optic wave modes. The proposed model may provide an efficient tool for modeling of the elastic metamaterial with complex microstructures.

Acknowledgments

This work was supported by the National Natural Science Foundation of China (11072031, 10832002, 10972036) and Natural Science Foundation EAGER program (1037569).

Appendix A. Components of the local strain tensor

The detailed components of the local strain tensor are:

$$\varepsilon_{22}^{3(k,l)} = \phi_{22}^{3(k,l)} + \frac{\partial(\bar{b} \cos \theta)}{\partial x_2} (\phi_{22}^{2(k,l)} - \phi_{22}^{3(k,l)}) + \frac{\partial(\bar{b} \sin \theta)}{\partial x_2} (\phi_{32}^{2(k,l)} - \phi_{32}^{3(k,l)}) \quad (\text{A.1})$$

$$\varepsilon_{33}^{3(k,l)} = \phi_{33}^{3(k,l)} + \frac{\partial(\bar{b} \cos \theta)}{\partial x_3} (\phi_{23}^{2(k,l)} - \phi_{23}^{3(k,l)}) + \frac{\partial(\bar{b} \sin \theta)}{\partial x_3} (\phi_{33}^{2(k,l)} - \phi_{33}^{3(k,l)}) \quad (\text{A.2})$$

$$\begin{aligned} \varepsilon_{23}^{3(k,l)} = \varepsilon_{32}^{3(k,l)} = & \frac{1}{2} (\phi_{23}^{3(k,l)} + \phi_{32}^{3(k,l)}) + \frac{1}{2} \frac{\partial(\bar{b} \cos \theta)}{\partial x_3} (\phi_{22}^{2(k,l)} - \phi_{22}^{3(k,l)}) \\ & + \frac{1}{2} \frac{\partial(\bar{b} \sin \theta)}{\partial x_3} (\phi_{32}^{2(k,l)} - \phi_{32}^{3(k,l)}) + \frac{1}{2} \frac{\partial(\bar{b} \cos \theta)}{\partial x_2} (\phi_{23}^{2(k,l)} - \phi_{23}^{3(k,l)}) + \frac{1}{2} \frac{\partial(\bar{b} \sin \theta)}{\partial x_2} (\phi_{33}^{2(k,l)} - \phi_{33}^{3(k,l)}). \end{aligned} \quad (\text{A.3})$$

Appendix B. Kinetic energy density and strain energy density

The kinetic energy density $T(X_2, X_3, t)$ in the continuum fields is

$$\begin{aligned} T(X_2, X_3, t) = T_{ave}^{(k,l)} = & \frac{1}{A_c} (T^{1(k,l)} + T^{3(k,l)}) = \frac{1}{A_c} \left(\frac{1}{2} \rho_1 A_1 [(\dot{u}_2)^2 + (\dot{u}_3)^2] \right. \\ & + \frac{1}{2} \rho_3 \sum_{\alpha=2}^3 \left[A_3 (\dot{v}_\alpha)^2 + (J_1 + I_3^m - 2J_{60}) (\dot{\phi}_{2\alpha}^3)^2 \right. \\ & \left. \left. + (J_2 + I_2^m - 2J_{70}) (\dot{\phi}_{3\alpha}^3)^2 + J_1 (\dot{\phi}_{2\alpha}^2)^2 + J_2 (\dot{\phi}_{3\alpha}^2)^2 + (2J_{60} - 2J_1) \dot{\phi}_{2\alpha}^3 \dot{\phi}_{2\alpha}^2 + (2J_{70} - 2J_2) \dot{\phi}_{3\alpha}^3 \dot{\phi}_{3\alpha}^2 \right] \right) \quad (\text{B.1}) \end{aligned}$$

where

$$\begin{aligned} I_2^m = \iint_{A_3} x_3^2 dA_3, \quad I_3^m = \iint_{A_3} x_2^2 dA_3, \quad J_1 = \iint_{A_3} \bar{b}^2 \cos^2 \theta dA_3, \\ J_2 = \iint_{A_3} \bar{b}^2 \sin^2 \theta dA_3, \quad J_{60} = \iint_{A_3} \bar{b} r \cos^2 \theta dA_3, \quad J_{70} = \iint_{A_3} \bar{b} r \sin^2 \theta dA_3. \end{aligned}$$

And the strain energy density $W(X_2, X_3, t)$ in the continuum fields is

$$\begin{aligned} W(X_2, X_3, t) = W_{ave}^{(k,l)} = & \frac{1}{A_c} (W^{s(k,l)} + W^{m(k,l)}) \\ = & \frac{1}{A_c} \left(K_2 [(\bar{v}_2 - \bar{u}_2)^2 + (b_1 \phi_{22}^2)^2 + (b_1 \phi_{32}^2)^2] + K_3 [(\bar{v}_3 - \bar{u}_3)^2 + (b_2 \phi_{33}^2)^2 + (b_2 \phi_{23}^2)^2] \right. \\ & + \frac{E_3}{2(1 - \nu_3^2)} \left[A_3 (\phi_{22}^3)^2 + A_3 (\phi_{33}^3)^2 + J_4 (\phi_{22}^2 - \phi_{22}^3)^2 \right. \\ & + J_5 (\phi_{33}^2 - \phi_{33}^3)^2 + J_6 (\phi_{32}^2 - \phi_{32}^3)^2 + J_6 (\phi_{23}^2 - \phi_{23}^3)^2 \\ & \left. \left. + 2J_7 \phi_{22}^3 (\phi_{22}^2 - \phi_{22}^3) + 2J_8 \phi_{33}^3 (\phi_{33}^2 - \phi_{33}^3) \right] \right) \end{aligned}$$

$$\begin{aligned}
 & + \frac{E_3 \nu_3}{1 - \nu_3^2} \left[A_3 \phi_{22}^3 \phi_{33}^3 + J_7 (\phi_{22}^2 - \phi_{22}^3) \phi_{33}^3 + J_8 (\phi_{33}^2 - \phi_{33}^3) \phi_{22}^3 \right. \\
 & \left. + J_6 (\phi_{22}^2 - \phi_{22}^3) (\phi_{33}^2 - \phi_{33}^3) + J_6 (\phi_{32}^2 - \phi_{32}^3) (\phi_{23}^2 - \phi_{23}^3) \right] \\
 & + \frac{E_3}{1 + \nu_3} \left\{ \frac{A_3}{4} (\phi_{23}^3 + \phi_{32}^3)^2 + \frac{1}{4} [J_6 (\phi_{22}^2 - \phi_{22}^3)^2 + J_6 (\phi_{33}^2 - \phi_{33}^3)^2 \right. \\
 & + J_4 (\phi_{23}^2 - \phi_{23}^3)^2 + J_5 (\phi_{32}^2 - \phi_{32}^3)^2 + 2J_6 (\phi_{22}^2 - \phi_{22}^3) (\phi_{33}^2 - \phi_{33}^3) \\
 & + 2J_6 (\phi_{32}^2 - \phi_{32}^3) (\phi_{23}^2 - \phi_{23}^3) + 2J_7 (\phi_{23}^2 - \phi_{23}^3) \phi_{33}^3 \\
 & \left. + 2J_8 (\phi_{32}^2 - \phi_{32}^3) \phi_{33}^3 + 2J_7 (\phi_{23}^2 - \phi_{23}^3) \phi_{32}^3 + 2J_8 (\phi_{32}^2 - \phi_{32}^3) \phi_{23}^3 \right\} \Bigg) \tag{B.2}
 \end{aligned}$$

where

$$\begin{aligned}
 J_4 &= \iint_{A_3} \frac{\bar{b}^2}{r^2} \sin^4 \theta \, dA_3, & J_5 &= \iint_{A_3} \frac{\bar{b}^2}{r^2} \cos^4 \theta \, dA_3, & J_6 &= \iint_{A_3} \frac{\bar{b}^2}{r^2} \sin^2 \theta \cos^2 \theta \, dA_3, \\
 J_7 &= \iint_{A_3} \frac{\bar{b}}{r} \sin^2 \theta \, dA_3, & J_8 &= \iint_{A_3} \frac{\bar{b}}{r} \cos^2 \theta \, dA_3.
 \end{aligned}$$

Appendix C. Governing equations

The sixteen governing equations of motion are:

$$\rho_1 A_1 \ddot{u}_2 + 2K_2 (\bar{u}_2 - \bar{v}_2) = 0 \tag{C.1}$$

$$\rho_1 A_1 \ddot{u}_3 + 2K_3 (\bar{u}_3 - \bar{v}_3) = 0 \tag{C.2}$$

$$\rho_3 A_3 \ddot{v}_2 + 2K_2 (\bar{v}_2 - \bar{u}_2) - A_c \frac{\partial \Gamma_{22}}{\partial X_2} - A_c \frac{\partial \Gamma_{32}}{\partial X_3} = 0 \tag{C.3}$$

$$\rho_3 A_3 \ddot{v}_3 + 2K_3 (\bar{v}_3 - \bar{u}_3) - A_c \frac{\partial \Gamma_{23}}{\partial X_2} - A_c \frac{\partial \Gamma_{33}}{\partial X_3} = 0 \tag{C.4}$$

$$\begin{aligned}
 & \rho_3 J_1 \ddot{\phi}_{22}^2 + \rho_3 (J_{60} - J_1) \ddot{\phi}_{22}^3 + 2b_1^2 K_2 \phi_{22}^2 + \frac{E_3}{1 - \nu_3^2} [J_4 (\phi_{22}^2 - \phi_{22}^3) + J_7 \phi_{22}^3] \\
 & + \frac{E_3 \nu_3}{1 - \nu_3^2} [J_7 \phi_{33}^3 + J_6 (\phi_{33}^2 - \phi_{33}^3)] + \frac{E_3}{2(1 + \nu_3)} [J_6 (\phi_{22}^2 - \phi_{22}^3) + J_6 (\phi_{33}^2 - \phi_{33}^3)] \\
 & - A_c \frac{2b_2}{d_3} \ln(\xi + \sqrt{1 + \xi^2}) \Gamma_{22} + A_c \frac{b_2 d_2}{d_3} \ln(\xi + \sqrt{1 + \xi^2}) \frac{\partial \Gamma_{22}}{\partial X_2} = 0 \tag{C.5}
 \end{aligned}$$

$$\begin{aligned}
 & \rho_3 J_1 \ddot{\phi}_{23}^2 + \rho_3 (J_{60} - J_1) \ddot{\phi}_{23}^3 + 2b_2^2 K_3 \phi_{23}^2 + \frac{E_3}{1 - \nu_3^2} [J_6 (\phi_{23}^2 - \phi_{23}^3)] \\
 & + \frac{E_3 \nu_3}{1 - \nu_3^2} [J_6 (\phi_{32}^2 - \phi_{32}^3)] + \frac{E_3}{2(1 + \nu_3)} [J_4 (\phi_{23}^2 - \phi_{23}^3) + J_6 (\phi_{32}^2 - \phi_{32}^3) \\
 & + J_7 \phi_{23}^3 + J_7 \phi_{32}^3] - A_c \frac{2b_2}{d_3} \ln(\xi + \sqrt{1 + \xi^2}) \Gamma_{23} + A_c \frac{b_2 d_2}{d_3} \ln(\xi + \sqrt{1 + \xi^2}) \frac{\partial \Gamma_{23}}{\partial X_2} = 0 \tag{C.6}
 \end{aligned}$$

$$\begin{aligned}
 & \rho_3 J_2 \ddot{\phi}_{32}^2 + \rho_3 (J_{70} - J_2) \ddot{\phi}_{32}^3 + 2b_1^2 K_2 \phi_{32}^2 + \frac{E_3}{1 - \nu_3^2} [J_6 (\phi_{32}^2 - \phi_{32}^3)] \\
 & + \frac{E_3 \nu_3}{1 - \nu_3^2} [J_6 (\phi_{23}^2 - \phi_{23}^3)] + \frac{E_3}{2(1 + \nu_3)} [J_5 (\phi_{32}^2 - \phi_{32}^3) + J_6 (\phi_{23}^2 - \phi_{23}^3) \\
 & + J_8 \phi_{23}^3 + J_8 \phi_{32}^3] - A_c \frac{2b_1}{d_2} \ln\left(\frac{1 + \sqrt{1 + \xi^2}}{\xi}\right) \Gamma_{32} + A_c \frac{b_1 d_3}{d_2} \ln\left(\frac{1 + \sqrt{1 + \xi^2}}{\xi}\right) \frac{\partial \Gamma_{32}}{\partial X_3} = 0 \tag{C.7}
 \end{aligned}$$

$$\begin{aligned}
 & \rho_3 J_2 \ddot{\phi}_{33}^2 + \rho_3 (J_{70} - J_2) \ddot{\phi}_{33}^3 + 2b_2^2 K_3 \phi_{33}^2 + \frac{E_3}{1 - \nu_3^2} [J_5 (\phi_{33}^2 - \phi_{33}^3) + J_8 \phi_{33}^3] \\
 & + \frac{E_3 \nu_3}{1 - \nu_3^2} [J_8 \phi_{22}^3 + J_6 (\phi_{22}^2 - \phi_{22}^3)] + \frac{E_3}{2(1 + \nu_3)} [J_6 (\phi_{33}^2 - \phi_{33}^3) + J_6 (\phi_{22}^2 - \phi_{22}^3)]
 \end{aligned}$$

$$-A_c \frac{2b_1}{d_2} \ln \left(\frac{1 + \sqrt{1 + \xi^2}}{\xi} \right) \Gamma_{33} + A_c \frac{b_1 d_3}{d_2} \ln \left(\frac{1 + \sqrt{1 + \xi^2}}{\xi} \right) \frac{\partial \Gamma_{33}}{\partial X_3} = 0 \quad (C.8)$$

$$\begin{aligned} \rho_3 (J_1 + I_3^m - 2J_{60}) \phi_{22}^{\ddot{3}} + \rho_3 (J_{60} - J_1) \phi_{22}^{\ddot{2}} + \frac{E_3}{1 - \nu_3^2} [A_3 \phi_{22}^3 + J_4 (\phi_{22}^3 - \phi_{22}^2)] \\ + J_7 \phi_{22}^2 - 2J_7 \phi_{22}^3] + \frac{E_3 \nu_3}{1 - \nu_3^2} [A_3 \phi_{33}^3 - J_7 \phi_{33}^3 + J_8 (\phi_{33}^2 - \phi_{33}^3) - J_6 (\phi_{33}^2 - \phi_{33}^3)] \\ + \frac{E_3}{2(1 + \nu_3)} [J_6 (\phi_{22}^3 - \phi_{22}^2) - J_6 (\phi_{33}^2 - \phi_{33}^3)] \\ + A_c \left[\frac{2b_2}{d_3} \ln (\xi + \sqrt{1 + \xi^2}) - 1 \right] \Gamma_{22} - A_c \left[\frac{b_2 d_2}{d_3} \ln (\xi + \sqrt{1 + \xi^2}) - \frac{d_2}{2} \right] \frac{\partial \Gamma_{22}}{\partial X_2} = 0 \end{aligned} \quad (C.9)$$

$$\begin{aligned} \rho_3 (J_1 + I_3^m - 2J_{60}) \phi_{23}^{\ddot{3}} + \rho_3 (J_{60} - J_1) \phi_{23}^{\ddot{2}} + \frac{E_3}{1 - \nu_3^2} [J_6 (\phi_{23}^3 - \phi_{23}^2)] \\ + \frac{E_3 \nu_3}{1 - \nu_3^2} [J_6 (\phi_{32}^3 - \phi_{32}^2)] + \frac{E_3}{2(1 + \nu_3)} [A_3 (\phi_{23}^3 + \phi_{32}^3) + J_4 (\phi_{23}^3 - \phi_{23}^2) \\ + J_6 (\phi_{32}^3 - \phi_{32}^2) + J_7 \phi_{23}^2 - 2J_7 \phi_{23}^3 - J_7 \phi_{32}^2 + J_8 (\phi_{32}^2 - \phi_{32}^3)] \\ + A_c \left[\frac{2b_2}{d_3} \ln (\xi + \sqrt{1 + \xi^2}) - 1 \right] \Gamma_{23} - A_c \left[\frac{b_2 d_2}{d_3} \ln (\xi + \sqrt{1 + \xi^2}) - \frac{d_2}{2} \right] \frac{\partial \Gamma_{23}}{\partial X_2} = 0 \end{aligned} \quad (C.10)$$

$$\begin{aligned} \rho_3 (J_2 + I_2^m - 2J_{70}) \phi_{32}^{\ddot{3}} + \rho_3 (J_{70} - J_2) \phi_{32}^{\ddot{2}} + \frac{E_3}{1 - \nu_3^2} [J_6 (\phi_{32}^3 - \phi_{32}^2)] \\ + \frac{E_3 \nu_3}{1 - \nu_3^2} [J_6 (\phi_{23}^3 - \phi_{23}^2)] + \frac{E_3}{2(1 + \nu_3)} [A_3 (\phi_{23}^3 + \phi_{32}^3) + J_5 (\phi_{32}^3 - \phi_{32}^2) \\ + J_6 (\phi_{23}^3 - \phi_{23}^2) + J_8 \phi_{32}^2 - 2J_8 \phi_{32}^3 - J_8 \phi_{23}^3 + J_7 (\phi_{23}^2 - \phi_{23}^3)] \\ + A_c \left[\frac{2b_1}{d_2} \ln \left(\frac{1 + \sqrt{1 + \xi^2}}{\xi} \right) - 1 \right] \Gamma_{32} - A_c \left[\frac{b_1 d_3}{d_2} \ln \left(\frac{1 + \sqrt{1 + \xi^2}}{\xi} \right) - \frac{d_3}{2} \right] \frac{\partial \Gamma_{32}}{\partial X_3} = 0 \end{aligned} \quad (C.11)$$

$$\begin{aligned} \rho_3 (J_2 + I_2^m - 2J_{70}) \phi_{33}^{\ddot{3}} + \rho_3 (J_{70} - J_2) \phi_{33}^{\ddot{2}} + \frac{E_3}{1 - \nu_3^2} [A_3 \phi_{33}^3 + J_5 (\phi_{33}^3 - \phi_{33}^2)] \\ + J_8 \phi_{33}^2 - 2J_8 \phi_{33}^3] + \frac{E_3 \nu_3}{1 - \nu_3^2} [A_3 \phi_{22}^3 - J_8 \phi_{22}^3 + J_7 (\phi_{22}^2 - \phi_{22}^3) + J_6 (\phi_{22}^3 - \phi_{22}^2)] \\ + \frac{E_3}{2(1 + \nu_3)} [J_6 (\phi_{33}^3 - \phi_{33}^2) - J_6 (\phi_{22}^2 - \phi_{33}^3)] \\ + A_c \left[\frac{2b_1}{d_2} \ln \left(\frac{1 + \sqrt{1 + \xi^2}}{\xi} \right) - 1 \right] \Gamma_{33} - A_c \left[\frac{b_1 d_3}{d_2} \ln \left(\frac{1 + \sqrt{1 + \xi^2}}{\xi} \right) - \frac{d_3}{2} \right] \frac{\partial \Gamma_{33}}{\partial X_3} = 0 \end{aligned} \quad (C.12)$$

$$\frac{\partial \bar{v}_2}{\partial X_2} - \frac{2b_2}{d_3} \ln (\xi + \sqrt{1 + \xi^2}) \left(\phi_{22}^2 - \phi_{22}^3 + \frac{d_2}{2} \frac{\partial \phi_{22}^2}{\partial X_2} - \frac{d_2}{2} \frac{\partial \phi_{22}^3}{\partial X_2} \right) - \phi_{22}^3 - \frac{d_2}{2} \frac{\partial \phi_{22}^3}{\partial X_2} = 0 \quad (C.13)$$

$$\frac{\partial \bar{v}_3}{\partial X_2} - \frac{2b_2}{d_3} \ln (\xi + \sqrt{1 + \xi^2}) \left(\phi_{23}^2 - \phi_{23}^3 + \frac{d_2}{2} \frac{\partial \phi_{23}^2}{\partial X_2} - \frac{d_2}{2} \frac{\partial \phi_{23}^3}{\partial X_2} \right) - \phi_{23}^3 - \frac{d_2}{2} \frac{\partial \phi_{23}^3}{\partial X_2} = 0 \quad (C.14)$$

$$\frac{\partial \bar{v}_2}{\partial X_3} - \frac{2b_1}{d_2} \ln \left(\frac{1 + \sqrt{1 + \xi^2}}{\xi} \right) \left(\phi_{32}^2 - \phi_{32}^3 + \frac{d_3}{2} \frac{\partial \phi_{32}^2}{\partial X_3} - \frac{d_3}{2} \frac{\partial \phi_{32}^3}{\partial X_3} \right) - \phi_{32}^3 - \frac{d_3}{2} \frac{\partial \phi_{32}^3}{\partial X_3} = 0 \quad (C.15)$$

$$\frac{\partial \bar{v}_3}{\partial X_3} - \frac{2b_1}{d_2} \ln \left(\frac{1 + \sqrt{1 + \xi^2}}{\xi} \right) \left(\phi_{33}^2 - \phi_{33}^3 + \frac{d_3}{2} \frac{\partial \phi_{33}^2}{\partial X_3} - \frac{d_3}{2} \frac{\partial \phi_{33}^3}{\partial X_3} \right) - \phi_{33}^3 - \frac{d_3}{2} \frac{\partial \phi_{33}^3}{\partial X_3} = 0. \quad (C.16)$$

References

- [1] X. Hu, C.T. Chan, J. Zi, Two-dimensional sonic crystals with Helmholtz resonators, *Phys. Rev. E* 71 (2005) 055601(R).
- [2] X. Hu, C.T. Chan, Refraction of water waves by periodic cylinder arrays, *Phys. Rev. Lett.* 95 (2005) 154501.
- [3] Z. Liu, X. Zhang, Y. Mao, Y.Y. Zhu, Z. Yang, C.T. Chan, P. Sheng, Locally resonant sonic materials, *Science* 289 (2000) 1734–1736.
- [4] S. Yang, J.H. Page, Z. Liu, M.L. Cowan, C.T. Chan, P. Sheng, Ultrasound tunneling through 3D phononic crystals, *Phys. Rev. Lett.* 88 (2002) 104301.

- [5] Z. Hou, X. Fu, Y. Liu, Computational method to study the transmission properties of phononic crystals, *Phys. Rev. B* 70 (2004) 014304.
- [6] N. Fang, D. Xi, J. Xu, M. Ambati, W. Srituravanich, C. Sun, X. Zhang, Ultrasonic metamaterials with negative modulus, *Nature Mater.* 5 (2006) 452–456.
- [7] S. Gonella, A.C. To, W.K. Liu, Interplay between phononic bandgaps and piezoelectric microstructures for energy harvesting, *J. Mech. Phys. Solids* 57 (2009) 621–633.
- [8] X.N. Liu, G.K. Hu, G.L. Huang, C.T. Sun, Wave propagation characterization and design of two-dimensional elastic chiral metacomposite, *J. Vib. Acoust.* 330 (2011).
- [9] M. Kafesaki, E.N. Economou, Multiple scattering theory for 3D periodic acoustic composites, *Phys. Rev. B* 60 (1999) 11993.
- [10] X. Hu, K.M. Ho, C.T. Chan, J. Zi, Homogenization of acoustic metamaterials of Helmholtz resonators in fluid, *Phys. Rev. B* 77 (2008) 172301.
- [11] P. Sheng, *Introduction to Wave Scattering, Localization, and Mesoscopic Phenomena*, Academic, San Diego, 1995.
- [12] Z. Liu, C.T. Chan, P. Sheng, Analytic model of phononic crystals with local resonances, *Phys. Rev. B* 71 (2005) 014103.
- [13] J. Mei, Z. Liu, W. Wen, P. Sheng, Effective mass density of fluid–solid composites, *Phys. Rev. Lett.* 96 (2006) 024301.
- [14] Y. Wu, Y. Lai, Z.Q. Zhang, Effective medium theory for elastic metamaterials in two dimensions, *Phys. Rev. B* 76 (2007) 205313.
- [15] Z. Yang, J. Mei, M. Yang, N.H. Chan, P. Sheng, Membrane-type acoustic metamaterial with negative dynamic mass, *Phys. Rev. Lett.* 101 (2008) 204301.
- [16] X.M. Zhou, G.K. Hu, Analytic model of elastic metamaterials with local resonances, *Phys. Rev. B* 79 (2009) 195109.
- [17] Y. Ding, Z. Liu, C. Qiu, J. Shi, Metamaterial with simultaneously negative bulk modulus and mass density, *Phys. Rev. Lett.* 99 (2007) 093904.
- [18] M.G. Imhof, Multiple multipole expansions for elastic scattering, *J. Acoust. Soc. Am.* 100 (1996) 2969–2979.
- [19] G. Wang, X. Wen, J. Wen, L. Shao, Y. Liu, Two-dimensional locally resonant phononic crystals with binary structures, *Phys. Rev. Lett.* 93 (2004) 154302.
- [20] A. Khelif, P.A. Deymier, B. Djafari-Rouhani, J.O. Vasseur, L. Dobrzynski, Two-dimensional phononic crystal with tunable narrow pass band: application to a waveguide with selective frequency, *J. Appl. Phys.* 94 (2003) 1308.
- [21] D. Torrent, J. Sánchez-Dehesa, Anisotropic mass density by two-dimensional acoustic metamaterials, *New J. Phys.* 10 (2008) 023004.
- [22] X. Ao, C.T. Chan, Far-field image magnification for acoustic waves using anisotropic acoustic metamaterials, *Phys. Rev. E* 77 (2008) 025601.
- [23] J.R. Willis, Exact effective relations for dynamics of a laminated body, *Mech. Mater.* 41 (2009) 385–393.
- [24] J.R. Willis, Effective constitutive relations for waves in composites and metamaterials, *Proc. R. Soc. A* (2011), doi:10.1098/rspa.2010.0620.
- [25] A.L. Shuvalov, A.A. Kutsenko, A.N. Norris, O. Poncelet, Effective Willis constitutive equations for periodically stratified anisotropic elastic media, *Proc. R. Soc. A* 467 (2011) 1749–1769.
- [26] S. Nemat-Nasser, J.R. Willis, A. Srivastava, A.V. Amirkhizi, Homogenization of periodic elastic composites and locally resonant sonic materials, *Phys. Rev. B* 83 (2011) 104103.
- [27] M. Hirsekorn, P.P. Delsanto, Elastic wave propagation in locally resonant sonic material: comparison between local interaction simulation approach and modal analysis, *J. Appl. Phys.* 99 (2006) 124912.
- [28] Y. Gu, X. Luo, H. Ma, Low frequency elastic wave propagation in two dimensional locally resonant phononic crystal with asymmetric resonator, *J. Appl. Phys.* 105 (2009) 044903.
- [29] Cz. Wozniak, Refined macro-dynamics of periodic structures, *Arch. Mech.* 45 (1993) 295–304.
- [30] G.W. Milton, J.R. Willis, On modifications of Newton's second law and linear continuum elastodynamics, *Proc. R. Soc. A* 463 (2007) 855–880.
- [31] G.W. Milton, New metamaterials with macroscopic behavior outside that of continuum elastodynamics, *New J. Phys.* 9 (2007) 359.
- [32] J.J. Alibert, P. Seppecher, F. Dell'Isola, Truss modular beams with deformation energy depending on higher displacement gradients, *Math. Mech. Solids* 8 (2003) 51–73.
- [33] E. Cosserat, F. Cosserat, *Théorie des corps déformables*, A. Hermann et Fils, Paris, 1909.
- [34] A.C. Eringen, E.S. Suhubi, Nonlinear theory of simple micro-elastic solids-I, *Int. J. Eng. Sci.* 2 (1964) 189–203.
- [35] R.A. Toupin, Elastic materials with couple-stresses, *Arch. Ration. Mech. Anal.* 11 (1962) 385–414.
- [36] A.C. Eringen, *Microcontinuum Field Theories I: Foundations and Solids*, Springer-Verlag, New York, 1999.
- [37] R.D. Mindlin, Micro-structure in linear elasticity, *Arch. Ration. Mech. Anal.* 16 (1964) 51–78.
- [38] C.T. Sun, J.D. Achenbach, G. Herrmann, Continuum theory for a laminated medium, *J. Appl. Mech.* 53 (1968) 467–475.
- [39] G.L. Huang, C.T. Sun, Continuum modeling of solids with micro/nanostructures, *Philos. Mag.* 87 (2007) 3689–3707.
- [40] R. Zhu, H.H. Huang, G.L. Huang, C.T. Sun, Microstructure continuum modeling of an elastic metamaterial, *Int. J. Eng. Sci.* 49 (2011) 1477–1485.
- [41] J.R. Barber, *Elasticity*, third ed., Springer, Dordrecht, 2010.